collagen, and promote wound healing. Mol Ther. 2007; 15: 628-635.

19) Conget P, Rodriguez F, Kramer S, Allers C, Simon V, Palisson F, Gonzalez S, Yubero MJ: Replenishment of type VII collagen and re-epithelialization of chronically ulcerated skin after intradermal administration of allogeneic mesenchymal stromal cells in two patients with recessive dystrophic epidermolysis bullosa. Cytotherapy. 2010; 12: 429-431.

20) Ferrari G, Cusella-De Angelis G, Coletta M, Paolucci E, Stornaiuolo A, Cossu G, Mavilio F: Muscle regeneration by bone marrow-derived myogenic progenitors. Science. 1998; 279: 1528-1530.

21) Lagasse E, Connors H, Al-Dhalimy M, Reitsma M, Dohse M, Osborne L, Wang X, Finegold M, Weissman IL, Grompe M: Purified hematopoietic stem cells can differentiate into hepatocytes in vivo. Nat Med. 2000; 6: 1229-1234.

22) Inokuma D, Abe R, Fujita Y, Sasaki M, Shibaki A, Nakamura H, McMillan JR, Shimizu T, Shimizu H: CTACK/CCL27 accelerates skin regeneration via accumulation of bone marrow-derived keratinocytes. Stem cells (Dayton, Ohio). 2006; 24: 2810-2816.

23) Sasaki M, Abe R, Fujita Y, Ando S, Inokuma D, Shimizu H: Mesenchymal stem cells are recruited into wounded skin and contribute to wound repair by transdifferentiation into multiple skin cell type. J Immunol. 2008; 180: 2581-2587.

24) Nishie W, Sawamura D, Goto M, Ito K, Shibaki A, McMillan JR, Sakai K, Nakamura H, Olasz E, Yancey KB, Akiyama M, Shimizu H: Humanization of autoantigen. Nat Med. 2007; 13: 378-383.

25) Fujita Y, Abe R, Inokuma D, Sasaki M, Hoshina D, Natsuga K, Nishie W, McMillan JR, Nakamura H, Shimizu T, Akiyama M, Sawamura D, Shimizu H: Bone marrow transplantation restores epidermal basement membrane protein expression and rescues epidermolysis bullosa model mice. Proc Natl Acad Sci U S A. 2010; 107: 14345-14350.

26) Tolar J, Ishida-Yamamoto A, Riddle M, McElmurry RT, Osborn M, Xia L, Lund T, Slattery C, Uitto J, Christiano AM, Wagner JE, Blazar BR: Amelioration of epidermolysis bullosa by transfer of wild-type bone marrow cells. Blood. 2009; 113: 1167-1174.

27) Chino T, Tamai K, Yamazaki T, Otsuru S, Kikuchi Y, Nimura K, Endo M, Nagai M, Uitto J, Kitajima Y, Kaneda Y: Bone marrow cell transfer into fetal circulation can ameliorate genetic skin diseases by providing fibroblasts to the skin and inducing immune tolerance. Am J Pathol. 2008; 173: 803-814.

28) Wagner JE, Ishida-Yamamoto A, McGrath JA, Hordinsky M, Keene DR, Woodley DT, Chen M, Riddle MJ, Osborn MJ, Lund T, Dolan M, Blazar BR, Tolar J: Bone marrow transplantation for recessive dystrophic epidermolysis bullosa. N Engl J Med. 2010; 363: 629-639.

29) Goto M, Sawamura D, Ito K, Abe M, Nishie W, Sakai K, Shibaki A, Akiyama M, Shimizu H: Fibroblasts show more potential as target cells than keratinocytes in COL7A1 gene therapy of dystrophic epidermolysis bullosa. J Invest Dermatol. 2006; 126: 766-772.

30) Kopp J, Horch RE, Stachel KD, Holter W, Kandler MA, Hertzberg H, Rascher W, Campean V, Carbon R, Schneider H: Hematopoietic stem cell transplantation and subsequent 80% skin exchange by grafts from the same donor in a patient with Herlitz disease. Transplantation. 2005; 79: 255-256.

31) Sodani P, Isgro A, Gaziev J, Polchi P, Paciaroni K, Marziali M, Simone MD, Roveda A, Montuoro A, Alfieri C, De Angelis G, Gallucci C, Erer B, Isacchi G, Zinno F, Adorno G, Lanti A, Faulkner L, Testi M, Andreani M, Lucarelli G: Purified T-depleted, CD34+ peripheral blood and bone marrow cell transplantation from haploidentical mother to child with thalassemia. Blood. 2010; 115: 1296-1302.

32) Stern M, Ruggeri L, Mancusi A, Bernardo ME, de Angelis C, Bucher C, Locatelli F, Aversa F, Velardi A: Survival after T cell-depleted haploidentical stem cell transplantation is improved using the mother as donor. Blood. 2008; 112: 2990-2995.

Australasian Journal of Dermatology

Australasian Journal of Dermatology (2011) 52, e1–e4 doi: 10.1111/j.1440-0960.2010.00684.x

CASE REPORT

Autosomal dominant bullous dermolysis of the newborn associated with a heterozygous missense mutation p.G1673R in type VII collagen

John Frew,[1] Shueh W Lim,[3] Alfred Klausseger,[5] Chung W Chow,[4] Kim Tran,[2] John Su,[4] David Orchard,[4] George Varigos,[4] Daisuke Sawamura,[6] Wataru Nishie,[6] Hiroshi Shimizu[6] and Dédée F Murrell[1]

Departments of [1]Dermatology and [2]Anatomical Pathology, St George Hospital, University of New South Wales, Sydney, New South Wales, [3]Department of Dermatology, Austin Hospital, [4]Department of Dermatology, Royal Children's Hospital, Melbourne, Victoria, Australia; [5]EB-Haus, Salzburg, Austria; and [6]Department of Dermatology, Hokkaido University Graduate School of Medicine, Sapporo, Japan

ABSTRACT

Bullous dermolysis of the newborn is an inherited mechano-bullous disorder classed as a rare subtype of dystrophic epidermolysis bullosa. Fewer than 30 cases of bullous dermolysis of the newborn have been reported in the literature and the pathogenesis of the disease is poorly understood. Only a minority of cases have had pathogenic mutations identified. We present a case of a neonate born to non-consanguineous Caucasian parents with an exon 54 (c.5017G > A, p.G1673R) mutation reported as one mutant allele in a case of recessive dystrophic epidermolysis bullosa (generalized other).

Key words: bullous dermolysis of the newborn, genodermatoses, type VII collagen.

INTRODUCTION

Bullous dermolysis of the newborn (BDN) is an inherited mechano-bullous disorder classed as a rare subtype of dystrophic epidermolysis bullosa (DEB) and classified according to its inheritance as an autosomal dominant DEB-BDN or recessive DEB-BDN disorder.[1,2] It is characterized by blistering of the skin at birth in the setting of mechanical trauma, with subsequent improvement or complete resolution of symptoms over the ensuing months of life (OMIM 131705). Initial neonatal blistering can be widespread, involving the trunk and extremities. It occasionally affects the nails and mucous membranes and typically resolves by the end of the first year of life. Healing typically occurs without scarring, although permanent scarring has been reported.[2,3]

Fewer than 30 cases of BDN have been reported in the literature since the identification of the disease in 1985.[4] The pathogenesis of the disease is poorly understood; however, mutations in the collagen VII gene (*COL7A1*) have been implicated. Only a minority of cases have had pathogenic mutations identified.[2–8] The poor understanding of the disease process has detrimental implications in the accurate prognostication of neonatal blistering disorders.

We present a recent case of BDN involving a novel pathogenic *COL7A1* mutation. This mutation has also been described[6] in what was previously known as non-Hallopeau–Siemens recessive RDEB, now known as generalized other RDEB (RDEB-O).[1]

Main text

A male infant (Australasian EB Registry Patient Number: 234)[9] was born at 37 weeks gestation in November 2006 after an uncomplicated pregnancy to a mother of gravida 2, parity 0. The mother's first pregnancy underwent a

Abbreviations:

BDN	bullous dermolysis of the newborn
DEB	dystrophic epidermolysis bullosa
RDEB-O	generalized other recessive DEB

Correspondence: Professor Dédée Murrell, Department of Dermatology, Ground Floor, James Laws House, St George Hospital, Gray St, Kogarah, NSW 2217, Australia. Email: d.murrell@unsw.edu.au

John Frew, MB BS. Shueh W Lim, FACD. Alfred Klausseger, MSc. Chung W Chow, FRCPA. Kim Tran, FRCPA. John Su, FACD. David Orchard, FACD. George Varigos, FACD. Daisuke Sawamura, PhD. Wataru Nishie, PhD. Hiroshi Shimizu, PhD. Dédée F Murrell, FAAD.

Submitted 6 April 2010; accepted 6 June 2010.

Figure 1 Neonate demonstrating blisters at birth.

Figure 2 Blister caused by adhesive tape.

termination for reasons unrelated to the present case. The parents were non-consanguineous Caucasian Australians of British descent and had no previous children. The neonate was born with multiple erosions and erythematous patches that subsequently developed into confluent bullae on the trunk and extremities over the following hours (Fig. 1). The infant displayed neither mucosal involvement nor dysmorphic features and was otherwise systemically well.

Initial investigations of the proband included swabs of the eroded areas for microscopy, culture and sensitivity, Blood cultures were taken and intravenous flucloxacillin and gentamicin were initiated. On the second day of life, bullae were evident on the site where the cannula was secured to the arm with adhesive tape, and on other sites of mild mechanical trauma (Fig. 2). Subsequently, skin biopsies, light microscopy, immunofluorescence mapping (Fig. 3) and electron microscopy (Fig. 3) were undertaken.

Over the next 2 months, the severity and number of blisters and erosions decreased and previous blisters resolved without scarring. At 18 months of age, blistering had ceased and the only manifestations seen were milia on the palmar surface of the hands.

Differential diagnoses included Staph scalded skin syndrome, impetigo, toxic epidermal necrosis and epidermolysis bullosa.

Investigative results

Skin biopsies of the blisters showed sub-basal dermoepidermal separation below the level of the lamina densa. Immunofluorescence mapping showed reduced intensity staining with the LH7.2 antibody to collagen VII and basal as well as suprabasal collections of collagen VII (Fig. 3). Electron microscopy demonstrated a paucity of dermal anchoring fibrils and highly dilated endoplasmic reticula, forming stellate bodies within basal keratinocytes (Fig. 3).

The infant's genomic DNA from blood was found to be heterozygous for a missense mutation (Fig. 3) on exon 54 of *COL7A1* (c.5017G > A, p.G1673R) not previously described in BDN.[6,10] A second sequence variant on exon 5 was identified (c.592G > A, p.V198I); however, this was considered unlikely to be pathogenic. Both of these mutations were paternal in origin. In order to clarify the nature of the second sequence variant a polymorphism study was undertaken, screening 145 wildtype samples from a normal Caucasian European population for the c.592G > A, p. V198I sequence variant using polymerase chain reaction and direct sequencing. It was found in one of the 145 samples.

DISCUSSION

Bullous dermolysis of the newborn is characterized histologically by blister formation at the dermoepidermal junction, just below the level of the lamina densa. Dermal anchoring fibrils are reduced in number and quality, while epidermal collections of collagen VII are evident.[2] Electron microscopy reveals grossly dilated endoplasmic reticula of basal and suprabasal keratinocytes, known as 'stellate bodies'. The pathogenesis of BDN involves a defect in the intracytoplasmic packaging or transport of collagen VII in basal keratinocytes;[2] however, the underlying explanation of why specific mutations in *COL7A1* result in a transient as opposed to a permanent deficiency of anchoring fibrils is unclear. Only four *COL7A1* mutations have been previously described in BDN and none of the aforementioned mutations have been described in cases of recessive or dominant DEB.[10]

Previously described mutations in BDN include an acceptor splice site mutation in intron 35 of COL7A1 (4120-1G > C)8 and two cases involving glycine substitution mutations; p.G1522E[2] and a heterozygote for p.G1519D/p.G2251E.[5] In the latter case, p.G2251E was presumed to be the pathogenic mutation, as carriers for this polymorphism also displayed mild DEB characteristics such as nail dystro-

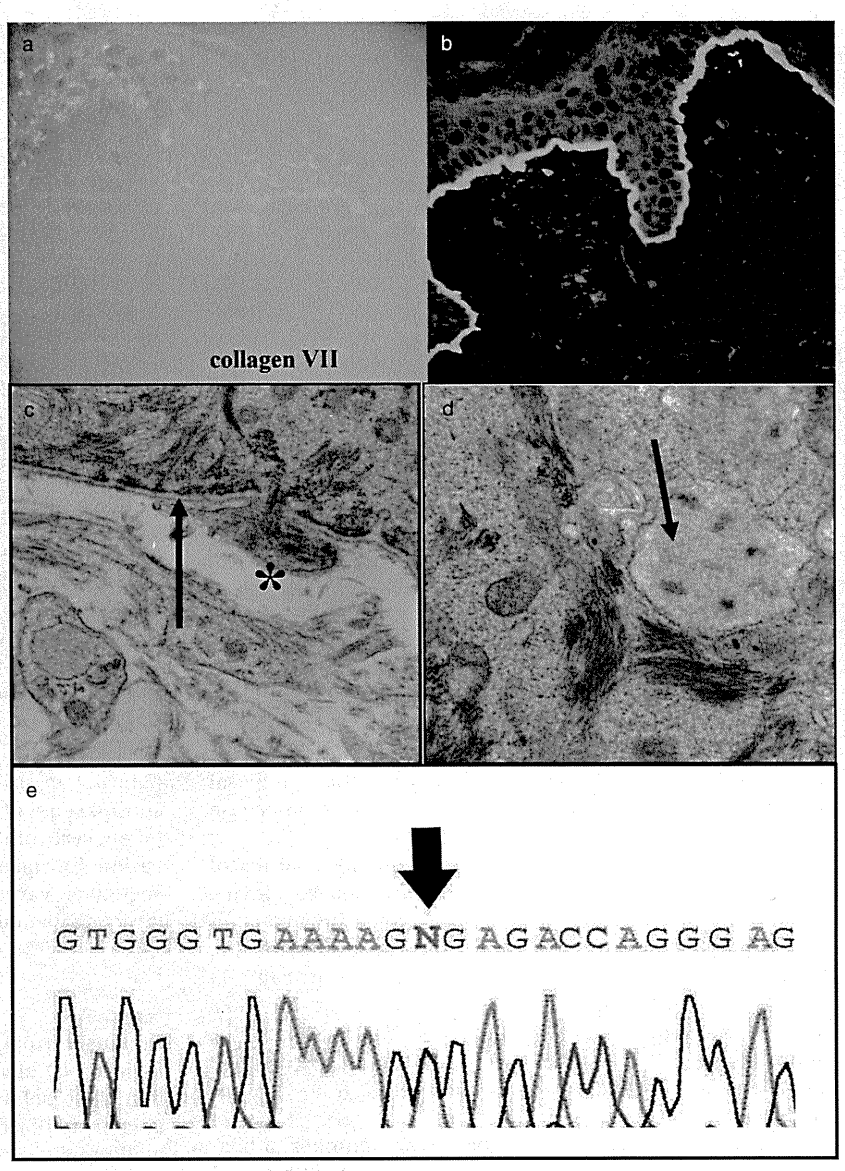

Figure 3 (a) Immunofluorescence mapping: stippled staining in the epidermis and lack of linear staining at the dermoepidermal junction, consistent with bullous dermolysis of the newborn (×20). (b) Control sample. (c) Electron microscopy showing the plane of cleavage (*) the basal lamina (arrow) and (d) typical keratinocyte 'stellate bodies' (arrow) (×10 000). (e) Genomic sequence data showing the missense mutation in exon 54 of *COL7A1*.

phy. The missense mutation in exon 54 (c.5017G > A, p.G1673R) has been previously described in another Caucasian family with RDEB-O;[6] however, the second mutation was not identified. Direct sequencing of exon 54 in 70 unrelated wildtype samples failed to identify the mutation (c.5017G > A, p.G1673R), indicating that it is not a neutral polymorphism. However, it may be possible that this glycine substitution is both a dominant and recessive mutation.

With regards to the exon 5 sequence variant, our polymorphism studies detected this genetic variation (V198I) once in 145 wildtype samples taken from a Caucasian European population. This suggests that the sequence variant is a rare single nucleotide polymorphism that is unlikely to be pathogenic. We postulate that this polymorphism is likely to lie on the same paternal allele of COL7A1, as the father and son both have the two mutations. Unfortunately, the mother declined genetic testing.

CONCLUSION

In summary, we present a case of autosomal dominant BDN in whom a linked *COL7A1* sequence variant has been identified which has been previously described in RDEB-O. Although the mechanism and pathogenesis of BDN is poorly understood, the fact that this mutation is also present in a previously described case of RDEB-O gives scope for hypotheses into how these two different diseases with different prognoses can coexist whilst sharing a pathogenic mutation. An increased understanding of the genotype–phenotype correlations in BDN may lead to a deeper

understanding of the mechanisms underlying defects in collagen VII production and transportation, which may in the future lead to therapeutic advancements for these disabling and disfiguring diseases.

REFERENCES

1. Fine J-D, Eady RA, Bauer E *et al.* The classification of inherited epidermolysis bullosa (EB): Report of the Third International Consensus Meeting on Diagnosis and Classification of EB. *J. Am. Acad. Dermatol.* 2008; **58**: 931–50.
2. Fassihi H, Diba VC, Wessagowit V *et al.* Transient bullous dermolysis of the newborn in three generations. *Br. J. Dermatol.* 2005; **153**: 1058–63.
3. Hanson S, Fine J-D, Levy ML. Three new cases of transient bullous dermolysis of the newborn. *J. Am. Acad. Derm.* 1999; **40**: 471–6.
4. Hashimoto K, Matsumoto H, Iacobelli D. Transient bullous dermolysis of the newborn. *Arch. Derm.* 1985; **121**: 1429–38.
5. Hammami-Hauasli N, Raghunath M, Kuster W *et al.* Transient bullous dermolysis of the newborn associated with compound heterozygosity for recessive and dominant COL7A1 mutations. *J. Invest. Dermatol.* 1998; **111**: 1214–19.
6. Dang N, Murrell DF. Mutation analysis and characterization of COL7A1 mutations in dystrophic epidermolysis bullosa. *Exp. Dermatol.* 2008; **17**: 553–68.
7. Nakano H, Toyomaki Y, Ohashi S *et al.* Novel COL7A1 mutations in a Japanese family with transient bullous dermolysis of the newborn associated with pseudosyndactyly. *Br. J. Dermatol.* 2007;**157**: 179–82.
8. Christiano AM, Fine J-D UJ. Genetic basis of dominantly inherited transient bullous dermolysis of the newborn: a splice site mutation in the type VII collagen gene. *J. Invest. Dermatol.* 1997; **109**: 811–14.
9. Kho YC, Agero AL, Rhodes LM *et al.* Epidemiology of EB in the antipodes: the Australasian EB registry with a focus on Herlitz junctional EB. *Arch. Dermatol.* 2010; **146**: 635–40.
10. Varki R, Sadowski S, Uitto J *et al.* Epidermolysis bullosa II. Type VII collagen mutations and phenotype-genotype correlations in the dystrophic subtypes. *J. Med. Genet.* 2007; **44**: 181–92.

available at www.sciencedirect.com

ScienceDirect

journal homepage: www.elsevier.com/locate/burns

Second harmonic generation and multiphoton microscopic detection of collagen without the need for species specific antibodies

Alice C.-H. Chen [a], *Celia McNeilly* [b], *Ashley P.-Y. Liu* [a], *Christopher J. Flaim* [b], *Leila Cuttle* [a], *Mark Kendall* [b], *Roy M. Kimble* [a], *Hiroshi Shimizu* [c], *James R. McMillan* [a,*]

[a] *The Centre for Children's Burns Research, Queensland Children's Medical Research Institute, Royal Children's Hospital, The University of Queensland, Brisbane, QLD 4029, Australia*

[b] *Australian Institute for Bioengineering and Nanotechnology, The University of Queensland, Brisbane, QLD 4072, Australia*

[c] *Department of Dermatology, Hokkaido University Graduate School of Medicine, Sapporo, Japan*

ARTICLE INFO

Article history:
Accepted 21 March 2011

Keywords:
Multi-photon microscope
Second harmonic generation
Collagen
Burn wound
Scar

ABSTRACT

High-resolution, high-contrast, three-dimensional images of live cell and tissue architecture can be obtained using second harmonic generation (SHG), which comprises non-absorptive frequency changes in an excitation laser line. SHG does not require any exogenous antibody or fluorophore labeling, and can generate images from unstained sections of several key endogenous biomolecules, in a wide variety of species and from different types of processed tissue. Here, we examined normal control human skin sections and human burn scar tissues using SHG on a multi-photon microscope (MPM). Examination and comparison of normal human skin and burn scar tissue demonstrated a clear arrangement of fibers in the dermis, similar to dermal collagen fiber signals. Fluorescence-staining confirmed the MPM-SHG collagen colocalization with antibody staining for dermal collagen type-I but not fibronectin or elastin. Furthermore, we were able to detect collagen MPM-SHG signal in human frozen sections as well as in unstained paraffin embedded tissue sections that were then compared with hematoxylin and eosin staining in the identical sections. This same approach was also successful in localizing collagen in porcine and ovine skin samples, and may be particularly important when species-specific antibodies may not be available. Collectively, our results demonstrate that MPM SHG-detection is a useful tool for high resolution examination of collagen architecture in both normal and wounded human, porcine and ovine dermal tissue.

1. Introduction

Multi-photon microscopy (MPM) is a nonlinear optical phenomenon that provides intrinsic optical sectioning of a specimen, and can provide high-resolution, high-contrast three-dimensional views of live cell and tissue architecture. Several extracellular matrix (ECM) components and key endogenous biomolecules can be visualized *in situ* without the need for tissue processing and staining, exogenous

* *Corresponding author at*: The University of Queensland, The Centre for Children's Burns Research, Queensland Children's Medical Research Institute, Level 4 Foundation Building, Royal Children's Hospital, Brisbane, QLD 4029, Australia. Tel.: +61 7 3636 9069; fax: +61 7 3365 5455.
E-mail address: j.mcmillan@uq.edu.au (J.R. McMillan).

0305-4179/$36.00.
doi:10.1016/j.burns.2011.03.013

antibody labeling or fluorophores. These include the autofluorescence from reducing coenzyme NAD(P)H, flavoproteins, keratin, melanin, and elastin [1]. In addition, detection of second-harmonic generation (SHG), the non-absorptive frequency changes in an excitation laser line can also be performed using MPM. SHG is a nonlinear optical effect that results in an emission wavelength that is half the excitation wavelength. Myosin, tubulin and collagen polymeric proteins have previously been studied using SHG [2–4]. Recent studies have used SHG signals to look at various skin disorders [1,5], and even immune cell migration in the skin [6]. Furthermore, it has also been shown to be a powerful tool in tissue engineering and can be used to monitor drug delivery [7,8].

In human skin, collagen makes up 70% of the dry weight of the dermis. Dermal fibroblasts are responsible for regulating the steady state synthesis of collagen deposition in normal skin. Several matrix metalloproteinases (MMPs 1, 2, 3, 8, 9, 13, 18) are responsible for collagen degradation, hence maintaining collagen-tissue equilibrium [9]. The balance between collagen production by (myo-)fibroblasts and collagen degradation by matrix metalloproteinases determines the precise collagen bundle size and hence dermal thickness during the process of post wounding dermal remodeling. After massive burn injury, granulation tissue formation and dermal remodeling takes place to fill and repair the damaged tissue. With deep dermal burns, this often results in an unsightly, raised hypertrophic scar. The scars are usually active for more than six months after injury, and mature after 18 months [10,11]. However, the orientation and distribution of collagen fiber arrangement at different time points after burn and in the pathophysiology of hypertrophic scar formation is still unclear.

It is well understood that hypertrophic scars have different collagen organization compared to normal skin, and that collections of parallel fibers and collagen nodules can be observed at different stages of scarring [12]. Several studies have been carried out to observe collagen architecture in hypertrophic scars, however many of the methods for detecting the presence of dermal collagens have been costly, time consuming and involved immunohistochemical antibody staining on tissue sections. In addition, studies using animal models often face difficulties finding species-specific antibodies, and there is also a need for *in vivo* imaging techniques to be developed. This study attempted to use an alternative higher-resolution microscopic method to assess collagen fiber arrangements in control and burn scar skin tissues. We examined human, porcine and ovine normal skin sections and compared these to dermal tissue at several different stages after burn using MPM based on SHG, and determined that MPM detection of SHG is a powerful tool for examination of collagen architecture in skin.

2. Materials and methods

2.1. *Sample preparation*

This research has been approved by the Royal Children's Hospital and Health Services District Human Research Ethics Committee and all studies were performed in accordance with the Helsinki declaration. Normal Human and scar tissue sections were collected from scar excision surgeries in the Royal Children's Hospital in Brisbane, Australia. Two surgically removed human foreskin tissues were also collected to represent normal human tissues (Table 1). Both donors were less than 12 months of age. The scar tissue donors were Asian girls aged 10 and 11 with burn scar tissue collected from the upper aspect of the foot and right thigh respectively approximately three years after the initial burn. All skin tissues collected were (1) fixed in 4% formalin, embedded in paraffin, and (2) embedded in OCT (embedding medium for frozen tissue to ensure Optimal Cutting Temperature) and snap frozen in liquid nitrogen, with sections cut at 5 microns (μm). Porcine normal and scar skin sections used in this experiment were first described by Cuttle et al. [13]. Burns were created on Large White juvenile pigs of approximately 8 weeks of age using 92 °C water for 15 s. A deep dermal partial thickness burn was created, with hypertrophic scarring observed after 99 days. Hypertrophic scar and normal skin samples were collected and fixed in 4% formalin, then embedded in paraffin. Skin samples of two pigs were used in this study. Ovine skin sections used in this experiment were first described by Fraser et al. [14]. Burns were created on Merino ewe fetuses at 80 days gestation using 66 °C water for 7 s and the tissue collected at 60 days post-burn. Merino ewe lambs were burned with 82 °C water for 10 s at 28–30 days of age and the tissue was collected 1 day later. Burn and normal skin samples were collected at several time points and fixed in 10% formalin then embedded in paraffin. Skin samples of three ovine fetuses and two ovine lambs were used in this study. All samples were examined in duplicate.

Table 1 – The origin, age and location of tissues used in this study.

Sample	Species	Age	Time after burn	Gender	Body site	Ethnic background/ species type
Normal 1	Human	Less than 1 year	–	Male	Foreskin	Caucasian
Normal 2	Human	Less than 1 year	–	Male	Foreskin	Caucasian
Scar 1	Human	10 years	40 months	Female	Ankle	Asian
Scar 2	Human	11 years	44 months	Female	Right thigh	Asian
Porcine normal/porcine scar	Porcine	22 weeks	99 days	Female	Right flank	Large White pig
Fetus normal/fetus burn	Ovine	140 days fetal gestation (term = 145–150 days)	60 days	–	Flank	Merino ewes
Lamb normal/lamb burn	Ovine	4 weeks	1 day	Male	Lower abdomen	Merino ewes

2.2. *Multiphoton microscopy*

A Zeiss 510 Meta NLO multi-photon microscope (Zeiss, North Ryde, NSW, Australia) was used to detect the SHG signal from both frozen sections and paraffin sections to determine the optimal spectral parameters for SHG excitation and signal collection for each technique (frozen or paraffin), species (human or pig) and specimen (normal skin or burn scar) types. Previous studies have used an excitation wavelength of 800–860 nm to detect collagen SHG [15–18], therefore here we used the BP 390–465 filter (collection wavelength of 390–465 nm) to cover the excitation wavelengths from 780 to 930 nm. Systematic checking of each excitation wavelength for optimal collagen visualization was performed by preliminary excitation wavelength screening at 10 nm intervals ranging from 790 nm to 920 nm. The 20× objective lens was used throughout this experiment (SHG and H&E visualizations). In order to confirm that the SHG signal detected was in fact specific for collagen, sequential SHG and Alexa488 fluorescent signals from immunohistochemically stained tissue sections were collected. Colocalization of SHG signal and Alexa488 was performed using the optimally determined SHG excitation/emission wavelength combination together with a second channel collecting the 500–550 nm emission from Alexa 488 (excited by a 488 nm laser). Zeiss AIM software was used to visualize the images. After SHG imaging both cryostat and paraffin sections were stained using routine hematoxylin and eosin (H&E) staining methods with acetone pre-treatment for cryostat sections [19].

2.3. *Indirect immunofluorescent staining*

For collagen I and fibronectin staining on frozen sections, slides were incubated in 10% goat serum (Millipore, CA, USA) blocking solution for 30 min, then incubated in a 1:100 dilution of collagen I monoclonal antibody ([COL-1] ab6308 Abcam,

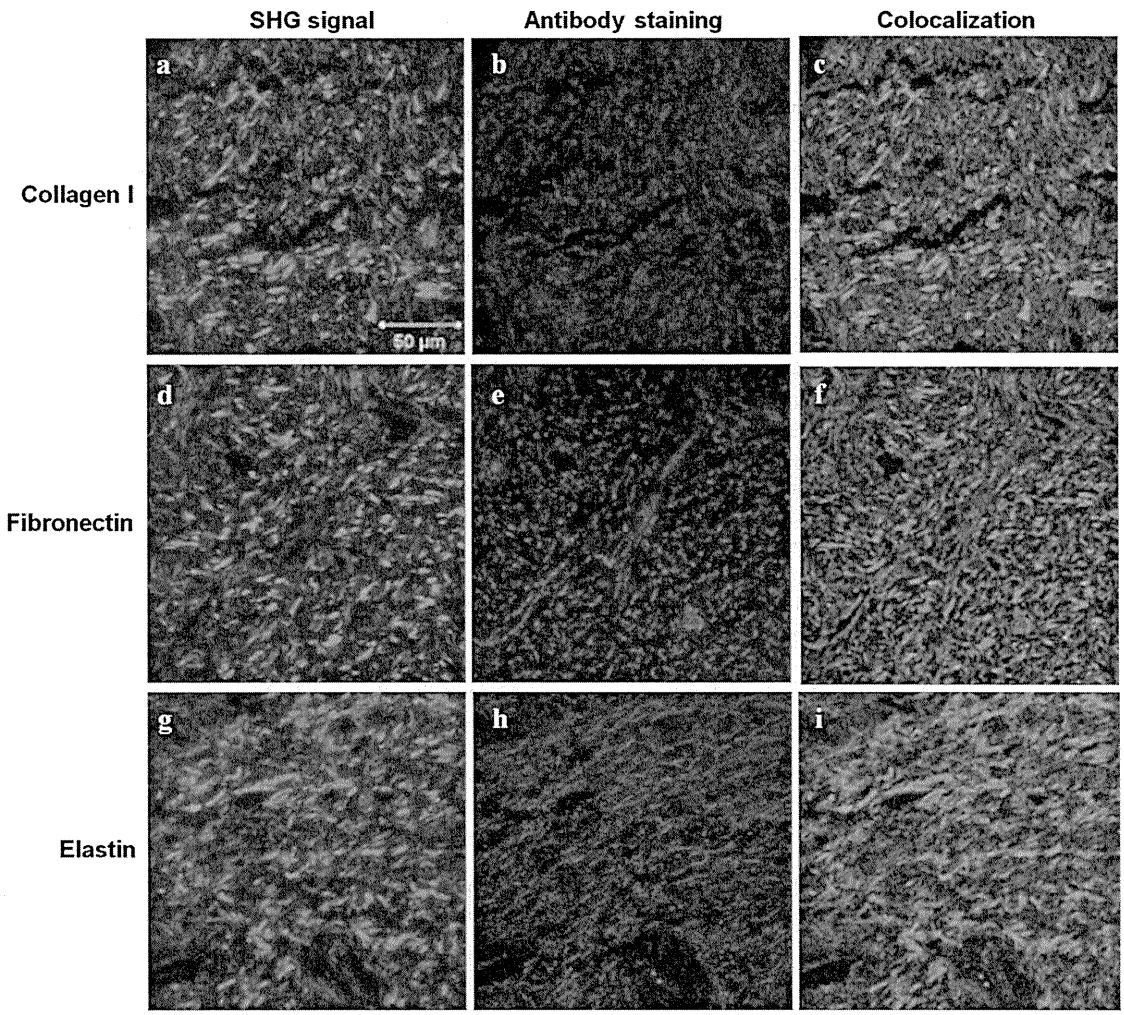

Fig. 1 – Co-localization of secondary harmonic image generation (SHG) and collagen I-, fibronectin- and elastin-antibody labeled human tissue sections show that the SHG signal closely co-localizes with collagen I-antibody staining, but not fibronectin or elastin. (a and d) SHG visualized on a frozen human *Normal* 1 tissue section, (g) SHG visualized on paraffin-embedded human *Normal* 1 tissue section, (b) collagen I-antibody labeled Alexa488 signal, (e) fibronectin-antibody labeled Alexa488 signal, (h) elastin-antibody labeled Alexa488 signal, and (c, f, and i) co-localization of SHG signal and antibody labeling.

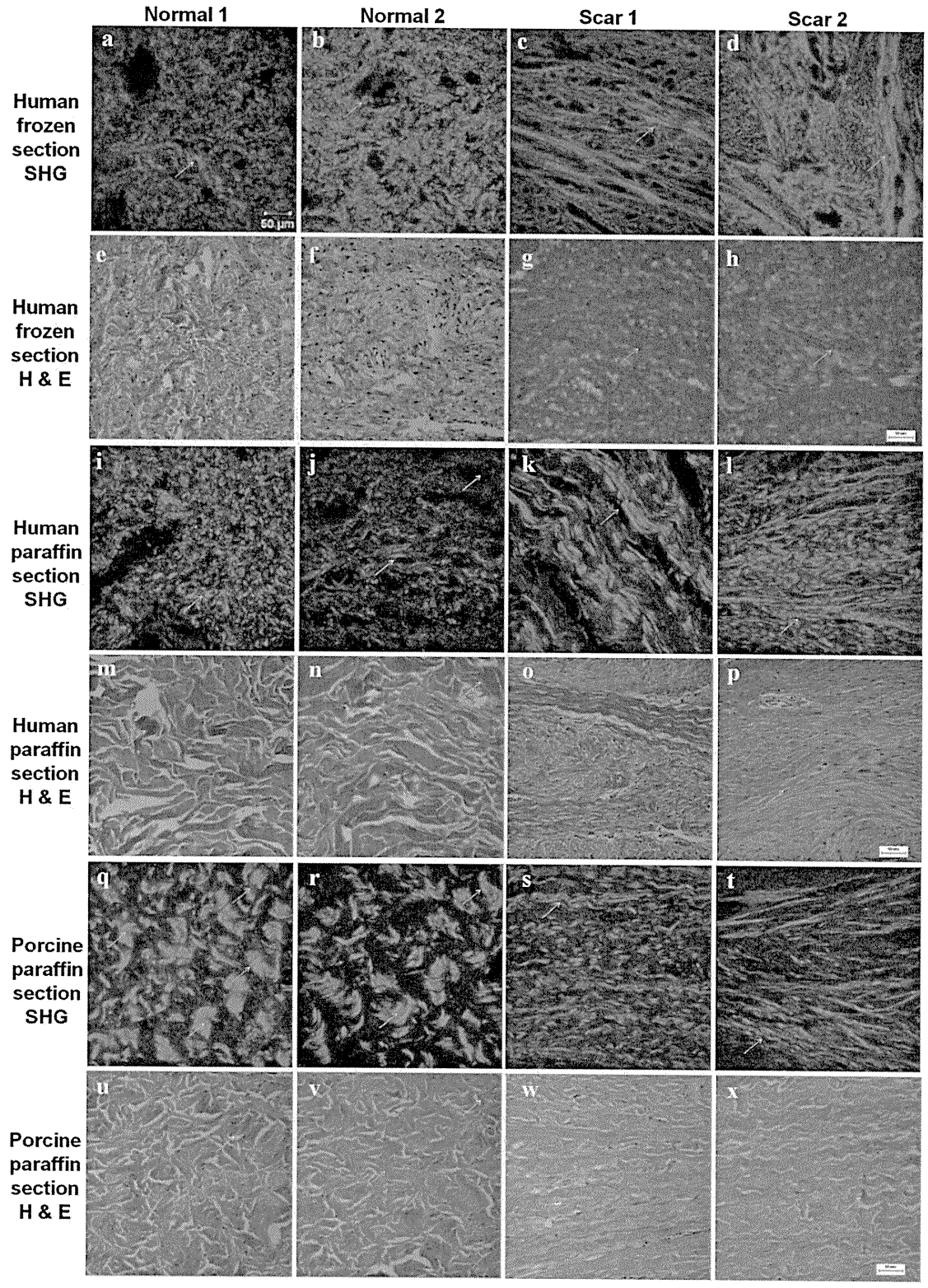

Fig. 2 – Human (a–p) and porcine skin (q–x) collagen architecture visualized using secondary harmonic image generation (SHG) and hematoxylin and eosin staining. All images were taken with the same microscope configuration/magnification to compare the differences in signal intensity and collagen arrangement between normal skin and scar tissue. The arrows in the control samples indicate the basket-weave arrangement in normal tissue, and highlight the elongated, wavy, undulating parallel collagen fibers observed in scar tissues. Collagen fiber bundles in H&E stained and SHG-visualized paraffin embedded sections

Cambridge, MA, USA) [20] or neat fibronectin supernatant monoclonal antibody HFN7.1 (DSHB, TX, USA) [21] at room temperature for 1 h in a humid atmosphere. After three washes in 0.1 M Dulbecco's phosphate buffered saline (PBS, five minutes per wash), slides were incubated in 1:500 Alexa Fluor 488 goat anti-mouse IgG antibody (Invitrogen, CA, USA) for 30 min at room temperature in a humid atmosphere in the dark. Microscope slides were washed three times in PBS, in distilled water and then coverslip mounted with Vectashield containing the nuclear staining agent, DAPI (1.5 μg/ml) (Vector Laboratories, Burlingame, CA, USA), and the coverslip edges sealed with non-fluorescent nail polish [22].

For elastin staining, as this antibody did not work in frozen sections, paraffin sections were dewaxed in xylene and processed through a descending ethanol series of washes, followed by trypsinization at 37 °C for 30 min using 0.2% trypsin (Gibco, CA, USA). Antibody permeabilization using 0.1% Triton X-100 (Merck, Australia) in PBS was performed at room temperature, incubated for 10 min with subsequent 30 min blocking in 10% normal goat serum (Millipore, CA, USA) in permeabilization solution at room temperature. Sections were incubated in 1:500 dilution monoclonal anti-elastin clone BA-4 (Sigma–Aldrich, MO, USA) [23] overnight at 4 °C. After three washes in PBS (five minutes each wash), slides were incubated in 1:500 Alexa Fluor 488 goat anti-mouse IgG antibody (Invitrogen, CA, USA) for 30 min at room temperature in the dark. Slides were then washed three times in PBS, then mounted with Vectashield with DAPI (Vector Laboratories, Burlingame, CA, USA) and the coverslips sealed with nail polish.

3. Results

To assess whether MPM is a viable alternative microscopic method to examine collagen deposition in control and burn scar tissues, we examined human normal skin and scar tissue using the MPM to detect SHG. Our results demonstrated that collagen SHG is best detected with lowest background noise at an excitation wavelength of 860 nm and an emission wavelength of 390–465 nm (data not shown). The localization of this putative collagen-SHG pattern was further compared to other dermal matrix components and was compared by dual channel colocalization with immunostaining using collagen I-, fibronectin- and elastin-antibody labeled tissue sections. The detected collagen-SHG signal showed a similar basket-weave arrangement pattern to collagen I antibody staining from normal human skin tissue (Fig. 1a and b), however the images did not completely overlap (Fig. 1c). Conversely, the putative collagen-SHG signal showed a completely different pattern when compared to fibronectin and elastin staining (Fig. 1f and i), with fibronectin demonstrating a finely organized nested pattern especially immediately below the epidermis (Fig. 1e), and elastin staining showed threads of thin fibers aligning in the same direction, parallel or perpendicular to the epidermis (Fig. 1h).

Two human control tissue samples and two human hypertrophic scar tissue samples were tested for SHG visualization and comparison with H&E staining at the optimal excitation wavelength of 860 nm, with an emission/collection wavelength of 390–465 nm. Collagen architecture in normal human dermis and burn hypertrophic scar tissue could be detected in both frozen (Fig. 2a–d) and paraffin sections (Fig. 2i–l) with similar signal intensity, however clearer collagen architecture was observed in the fixed paraffin-embedded sections (Fig. 2i–l). Collagen fibers in control foreskin sections were in a randomly but relatively loosely organized basket-weave-like arrangement, while scar tissue collagen fiber bundles comprised typically long fibers aligned in parallel or in an undulating pattern. Comparison with H&E stained cryostat and paraffin embedded sections confirmed the differences in collagen organization and packing observed by SHG between control and scar tissue. Comparison of H&E and SHG staining clearly demonstrated the higher density of collagen bundle packing in the scar samples in both cryostat (Fig. 2a–d versus e–h) and paraffin sections (Fig. 2i–l versus m–p). In general, SHG showed superior visualization of compacted collagen in bundles and the higher bundle density in human and porcine scar tissue compared to H&E stained sections. Furthermore, SHG provides significant improvements in collagen fiber resolution (see Fig. 2c and d, k and l, and s and t) that would allow clearer 3D image collection with the added benefit of ease of tissue preparation. Although the twisted or wavy characteristics of hypertrophic scar dermal collagen fibers were clearly observed in both scar sections, using both techniques (see arrows in Fig. 2k and o) no collagen nodules were visualized in these samples using either SHG or H&E visualization techniques.

The same approach was repeated using control porcine and hypertrophic scar paraffin-embedded sections to determine if different species exhibit similar optimal wavelengths for collagen SHG signal detection (see Fig. 2q–t). Our results show that porcine collagen SHG was best detected at excitation wavelength of 860 nm and an emission wavelength of 390–465 nm, which was identical to the detection of human dermal collagen (data not shown). Control porcine paraffin-embedded dermal tissue sections exhibited a stronger SHG signal intensity over the length of the shorter fibers (arrows in Fig. 2q and r) compared to scar tissue sections (Fig. 2s and t). Similar to human collagen architecture, control porcine dermis also demonstrated a basket-weave arrangement, while scar tissue exhibited extended, long wavy collagen fibers aligned in parallel with the epidermis (Fig. 2s and t). Again, H&E stained paraffin embedded sections confirmed the differences observed using SHG in collagen bundle distribution, length and packing between pig control and scar tissue samples.

exhibited identical distribution, length and packing patterns between human and porcine control and scar tissue samples. However, upon closer comparison SHG visualization exhibited increased resolution and clarity of individual collagen bundles, especially in scar tissue from all species examined (c and d, k and l, and s and t).

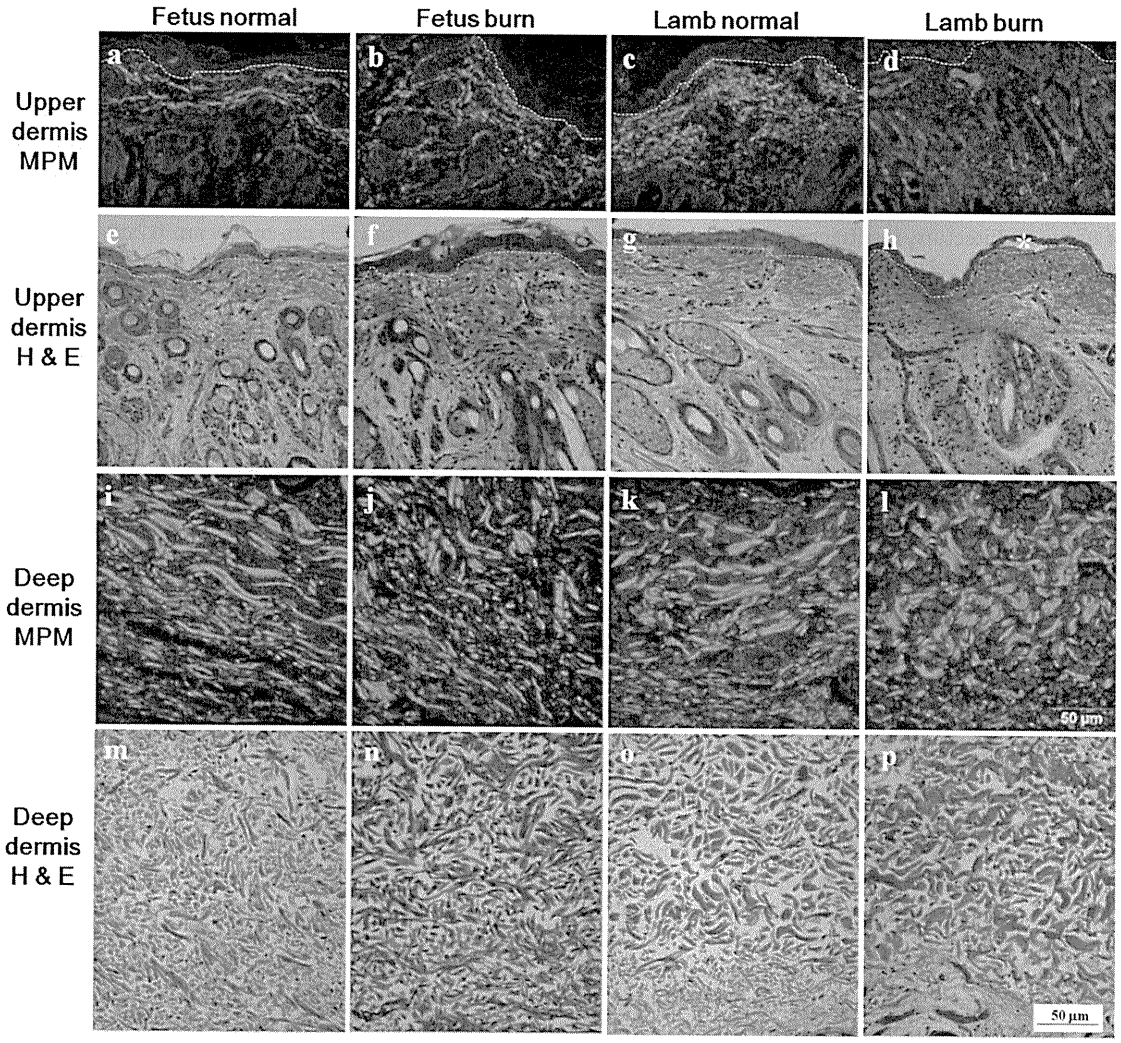

Fig. 3 – Ovine fetus and lamb skin collagen architecture visualized using secondary harmonic generation (upper dermal a–d; lower dermal staining i–l) and hematoxylin and eosin staining (upper dermal e–h; lower dermal staining m–p) in paraffin embedded sections. All images were taken with the same microscope configuration/magnification to compare the differences in signal intensity and collagen distribution arrangement between normal skin and skin after burn. The upper dermal field of view is predominantly comprised of wool follicles with a decreased presence of collagen lower in the mid-dermal tissue. The dashed lines indicate the epidermal-dermal junction with one figure showing epidermal separation after burn wounding (asterisk in h). The H&E stained paraffin embedded sections confirmed the more subtle differences observed using SHG in collagen bundle distribution, length and packing between ovine control and burn tissue samples.

Ovine collagen fibers were also successfully detected in both normal and burn tissue using the same MPM excitation and emission detection settings (Fig. 3). Thin collagen fibers were detected in the papillary dermis (just beneath the dashed lines Fig. 3a and b) of ovine normal control fetal tissue at 140 days gestation (term is 145–150 days) and fetal burn tissue after 60 days post-wounding normal control as well as in lamb tissue (Fig. 3c and d). Thick, SHG-bright collagen bundles were detected in both normal and burn tissues in fetal and lamb deep dermis that correlated with more eosinophilic collagen bundles in H&E sections of burn tissue (Fig. 3m and o verses n and p). Unlike human and porcine normal skin, the collagen architecture in ovine deep dermis showed relatively longer collagen bundles parallel-aligned in a wavy pattern, but the long, continuous parallel collagen architecture seen in human and porcine scar tissue was not observed in either the adult or fetal ovine tissue. Ovine fetal deep dermis at 60 days post burn demonstrated similar looking collagen bundles to normal control fetal skin (Fig. 3i versus j), however in contrast the collagen bundles were less regularly aligned in parallel. In addition, at 1 day after burn, thick collagen bundles were still visualized in the lamb acute burn deep dermis, but in a much shorter and curled form (Fig. 3i and p).

4. Discussion

Second harmonic generation detection using MPM has been widely used in various dermatological studies in the last few years [15,17,18,24]. It is a non-invasive, high resolution and high contrast laser microscopic technique that allows observation of tissue architecture, identification of skin pathology, and monitoring of drug delivery. Many dermatological studies often require immunohistochemical staining to observe different compartments of skin structure, and these methods include the most commonly used hematoxylin and eosin staining, Masson's Trichrome staining and Sirius red staining viewed using various forms of light microscopy. Antibody-labeled tissue sections or cells viewed by fluorescent or confocal laser microscopy are also frequently used to detect the distribution of specific proteins during molecular trafficking. Transmission electron microscopy can give a high magnification ultrastructural view of the tissue structure, however it is a very slow and time consuming method. Most of these methods require immunohistochemical staining, and are hence time consuming and relatively labor intensive. Second harmonic generation detection using MPM has been used to examine several dermatological conditions including studies observing melanin distribution [1]. The major strength of the SHG detection method is that no immunohistochemical staining is required; therefore long-term monitoring can be performed on the same tissue area without the possibility of image degradation or the need to take skin biopsies. This study demonstrates the feasibility of MPM application to detect collagen SHG in human, porcine and ovine burn tissues, for comparison with normal or control skin.

To verify that the SHG signal detected using MPM was collagen, colocalization of SHG and collagen I by immunohistochemical staining was performed. Although the two signals have similar patterns, the signals did not entirely overlap. One explanation is that a large proportion of the SHG signal detected was collagen III instead of or as well as collagen I. In normal human skin, the collagen I to collagen III ratio is about 3:1, however after burn, the ratio can dramatically alter to 2:1 [25]. After the gradual process of tissue remodeling, collagen III gets replaced by collagen I. Cuttle et al. [26] has described a method for detecting different collagen subtypes in burn tissues using Sirius red staining and polarization microscopy. Thicker and more closely packed collagen fibers such as collagen I exhibited an intense yellow or red birefringence, while relatively thin and looser-packed fibrils such as collagen III often showed a weaker, green tinged birefringence [27]. Although the SHG detection method cannot differentiate between different collagen subtypes, this non-invasive technique still benefits dermatological studies as there are no concerns about sample bleaching. Unfortunately, both the Sirius red method and the SHG collagen detection methods are dependent on collagen fiber density. Newly forming collagen I may be incorrectly identified as collagen III using the Sirius red method, and weak signals from thin fibrils could similarly be missed using the SHG detection method. The observation of mature scars would be expected to exhibit less variability using the SHG detection method, as examination of total collagen architecture is more important than being able to differentiate between different collagen types, and collagen fibers in mature scar would be of sufficient thickness to allow for sufficiently sensitive SHG detection. One advantage of SHG is in examining total global collagen fiber arrangement and architecture rather than detecting collagen subtypes.

Various studies recently published have used excitation wavelengths from 800 nm to 860 nm with an emission wavelength from 393 nm to 436 nm [17,18,24,28]. Our results show that the best SHG signal is detected at an excitation wavelength of 860 nm using the emissions filter that collects laser signals from 390 nm to 465 nm regardless of the tissue processing technique or species tissue origin. Previously, Chen et al. [18] have described the detection of SHG in human hypertrophic scars using 3-dimentiional modeling and Z-stacking methods, and have shown that collagen SHG signal intensity in normal tissue was roughly 1.5 times that in the hypertrophic scar tissue. In Fig. 2, our data did not demonstrate any difference in SHG signal intensity between normal and hypertrophic scar tissues in human samples. This could be due to the difference in sample age such that collagen fibers in children less than one year of age may be thinner and arranged in a different manner compared to teenagers/adolescents. However, it is very difficult to obtain age-, sex-, ethnic background- and body site-matched control human dermal tissue and foreskin tissue was our best option to use as a control in this study.

In this study, although our tissue samples were only 5 μm thick, we demonstrated similar collagen architecture described by Linares et al. [12] and Chen et al. [18] and this was confirmed by subsequent collagen fiber observations using hematoxylin and eosin (H&E) stained tissue in identical samples examined by SHG. Normal dermal architecture shows randomly oriented collagen fibers, while hypertrophic scars show elongated collagen bundles of undulating fibers. No obvious collagen nodules were detected in the hypertrophic scar tissues, possibly due to the relatively young age of the scars and the different body sites, and therefore differences in amounts of collagen cross-linkage and packing. Furthermore, there was a greater frequency of collagen with a more nested arrangement in human *Scar* sample 2 compared to human *Scar* sample 1. Again, this may be due to a slightly greater maturation of Scar 2 leading to changes in scar morphology or the different body sites that the scars were formed.

Among the various animal models used in skin wound and particularly burns research, the pig burn model is the most similar to human burn wounds in terms of skin structure, scale, composition, physiology and reaction to injury [29–33]. As shown in Fig. 2, the collagen architecture in porcine skin tissue was similar to that in human tissue, although each of the basket-weave collagen arrangements in normal porcine skin were more widely spaced compared to control human skin, which could be due to the differences in body size or site. Similar but less high resolution changes in collagen bundles were also detected in H&E stained sections in all species examined. Our results therefore provide further evidence that the porcine model is suitable for SHG collagen analysis. Although the ovine model is often used in fetal studies, the lack of species-specific antibodies can limit research using these animals as models. Our results demonstrated that SHG detection using MPM was a quick and powerful method to

study collagen in the ovine model. It was sensitive enough to identify thin collagen fibers in ovine fetal dermal tissue and thin or newly formed collagen fibers after burn as well as the morphological changes occurring in thick, deep dermal collagen bundles. Our success in detecting SHG in porcine and ovine dermal tissues shows the potential of applying this method to study collagen deposition in various diseases and animal models. Other researchers have validated the use of SHG detection in mouse skin and after lung fibrosis [16,34], further demonstrating the potential of SHG detection in dermatological research and research into dermal scarring.

This study demonstrated that high resolution collagen architecture in human, porcine and ovine tissue samples can be detected using SHG and MPM without the need for immunofluorescent staining on frozen tissue or paraffin-embedded tissue sections. Although embedding artifacts present in cryostat and paraffin-embedded sections can still be seen to a lesser extent, tissue architecture using the paraffin-embedded method is better preserved and the samples can be kept for longer periods with only simple storage requirements. Our study highlights the future potential for *in vivo* three-dimensional SHG monitoring of clinical patients to examine collagen architecture from an early stage after injury to identify any early pathogenic signs of hypertrophic scar formation. However, while the benefit and usefulness of *in vivo* application of MPM collagen assessment is theoretically possible, there still remain several issues affecting its usefulness for imaging in living animals. These include the ability of keeping the animals from moving to allow adequate image collection, and secondly the limitations in penetration of MPM microscopy to visualize deep into scar tissue. This method is highly sensitive to movements such as respiratory or involuntary nervous reflex movements, and the imaging depth of MPM in skin is only limited to about 200 μm. Therefore, to allow this method to work in live animal or clinical patients, scanning rates and imaging depth will have to be significantly improved through better the microscope design. Other than its clinical use, this approach also benefits dermatological research that involves animal models or human patients when species-specific antibodies are unavailable and painful biopsies have been refused. It can be an efficient technique clinically, as well as for histologically preserved tissue samples. Future studies should be carried out using this approach to examine a larger sample size of pathogenic scars compared to control tissue, to identify the key differences in collagen fiber organization and potentially the complex pathomechanisms of hypertrophic scarring.

Conflict of interest

The authors have no conflict of interest.

Acknowledgements

We would like to thank all the participants involved in this study. This work was funded by the Royal Children's Hospital Foundation and a New Staff Start Up Grant from The University of Queensland and by a grant-in-aid to J.R.M. from the Health and Labor Sciences Research Grant (research into specific diseases) H17-Saisei-12 to Hokkaido University (Japan). A.C.-H.C. is a recipient of The University of Queensland Australian Postgraduate Award scholarship. The fibronectin hybridoma supernatant HFN7.1 developed/donated by R.J. Klebe was obtained from the Developmental Studies Hybridoma Bank, developed under the auspices of the National Institute of Child Health and Development (NICHD) and maintained by the University of Iowa, Department of Biological Sciences, Iowa City, IA 52242, United States.

REFERENCES

[1] Konig K, Riemann I. High-resolution multiphoton tomography of human skin with subcellular spatial resolution and picosecond time resolution. J Biomed Opt 2003;8(July (3)):432–9.
[2] Freund I, Deutsch M, Sprecher A. Connective tissue polarity. Optical second-harmonic microscopy, crossed-beam summation, and small-angle scattering in rat-tail tendon. Biophys J 1986;50(October (4)):693–712.
[3] Kim BM, Eichler J, Da Silva LB. Frequency doubling of ultrashort laser pulses in biological tissues. Appl Opt 1999;38(December (34)):7145–50.
[4] Kim BM, Eichler J, Reiser KM, Rubenchik AM, Da Silva LB. Collagen structure and nonlinear susceptibility: effects of heat, glycation, and enzymatic cleavage on second harmonic signal intensity. Lasers Surg Med 2000;27(4): 329–35.
[5] Campagnola PJ, Millard AC, Terasaki M, Hoppe PE, Malone CJ, Mohler WA. Three-dimensional high-resolution second-harmonic generation imaging of endogenous structural proteins in biological tissues. Biophys J 2002;82(January (1 Pt 1)):493–508.
[6] Roediger B, Ng LG, Smith AL, de St Groth BF, Weninger W. Visualizing dendritic cell migration within the skin. Histochem Cell Biol 2008;130(December (6)):1131–46.
[7] Schenke-Layland K, Riemann I, Damour O, Stock UA, Konig K. Two-photon microscopes and in vivo multiphoton tomographs—powerful diagnostic tools for tissue engineering and drug delivery. Adv Drug Deliv Rev 2006;58(September (7)):878–96.
[8] Konig K, Ehlers A, Stracke F, Riemann I. In vivo drug screening in human skin using femtosecond laser multiphoton tomography. Skin Pharmacol Physiol 2006;19(2):78–88.
[9] Raffetto JD, Khalil RA. Matrix metalloproteinases in venous tissue remodeling and varicose vein formation. Curr Vasc Pharmacol 2008;6(July (3)):158–72.
[10] Schwanholt CA, Ridgway CL, Greenhalgh DG, Staley MJ, Gaboury TJ, Morress CS, et al. A prospective study of burn scar maturation in pediatrics: does age matter? J Burn Care Rehabil 1994;15(September–October (5)):416–20.
[11] Rochet JM, Zaoui A. Burn scars: rehabilitation and skin care. Rev Prat 2002;52(December (20)):2258–63.
[12] Linares HA, Kischer CW, Larson DL, Dobrkovs M. Histiotypic organization of hypertrophic scar in humans. J Invest Dermatol 1972;59(October (4)):323–31.
[13] Cuttle L, Kempf M, Phillips GE, Mill J, Hayes MT, Fraser JF, et al. A porcine deep dermal partial thickness burn model with hypertrophic scarring. Burns 2006;32(7):806–20.
[14] Fraser JF, Cuttle L, Kempf M, Phillips GE, O'Rourke PK, Choo K, et al. Deep dermal burn injury results in scarless wound healing in the ovine fetus. Wound Repair Regen 2005;13(March–April (2)):189–97.

[15] Yeh AT, Kao BS, Jung WG, Chen ZP, Nelson JS, Tromberg BJ. Imaging wound healing using optical coherence tomography and multiphoton microscopy in an in vitro skin-equivalent tissue model. J Biomed Opt 2004;9(March–April (2)):248–53 [article].
[16] Pena AM, Fabre A, Debarre D, Marchal-Somme J, Crestani B, Martin JL, et al. Three-dimensional investigation and scoring of extracellular matrix remodeling during lungfibrosis using multiphoton microscopy. Microsc Res Tech 2007;70(February (2)):162–70 [article].
[17] Da Costa V, Wei R, Lim R, Sun CH, Brown JJ, Wong BJF. Nondestructive imaging of live human keloid and facial tissue using multiphoton microscopy. Arch Facial Plast Surg 2008;10(January–February (1)):38–43 [article].
[18] Chen G, Chen J, Zhuo S, Xiong S, Zeng H, Jiang X, et al. Nonlinear spectral imaging of human hypertrophic scar based on two-photon excited fluorescence and second-harmonic generation. Br J Dermatol 2009;161(July (1)):48–55 [article].
[19] Bancroft JD, Stevens A. Theory and practice of histological techniques. Churchill Livingstone: London; 1996.
[20] Kidd KR, Williams SK. Laminin-5-enriched extracellular matrix accelerates angiogenesis and neovascularization in association with ePTFE. J Biomed Mater Res A 2004;69(May (2)):294–304.
[21] Schoen RC, Bentley KL, Klebe RJ. Monoclonal antibody against human fibronectin which inhibits cell attachment. Hybridoma 1982;1(2):99–108.
[22] McMillan JR, McGrath JA, Pulkkinen L, Kon A, Burgeson RE, Ortonne JP, et al. Immunohistochemical analysis of the skin in junctional epidermolysis bullosa using laminin 5 chain specific antibodies is of limited value in predicting the underlying gene mutation. Br J Dermatol 1997;136(June (6)):817–22.
[23] Wrenn DS, Griffin GL, Senior RM, Mecham RP. Characterization of biologically active domains on elastin: identification of a monoclonal antibody to a cell recognition site. Biochemistry 1986;25(September (18)):5172–6.
[24] Lu KC, Chen JX, Zhuo SM, Zheng LQ, Jiang XS, Zhu XQ, et al. Multiphoton laser scanning microscopy of localized scleroderma. Skin Res Technol 2009;15(November (4)): 489–95 [article].
[25] Prockop DJ, Kivirikko KI, Tuderman L, Guzman NA. Biosynthesis of collagen and its disorders, 1. N Engl J Med 1979;301(1):13–23 [review].
[26] Cuttle L, Nataatmadja M, Fraser JF, Kempf M, Kimble RM, Hayes MT. Collagen in the scarless fetal skin wound: detection with picrosirius-polarization. Wound Repair Regen 2005;13(March–April (2)):198–204.
[27] Montes GS, Junqueira LC. The use of the Picrosirius-polarization method for the study of the biopathology of collagen. Mem Inst Oswaldo Cruz 1991;86(Suppl. 3):1–11.
[28] Chen JX, Lee A, Zhao JH, Wang HQ, Lui H, McLean DI, et al. Spectroscopic characterization and microscopic imaging of extracted and in situ cutaneous collagen and elastic tissue components under two-photon excitation. Skin Res Technol 2009;15(November (4)):418–26 [article].
[29] Montagna W, Yun JS. The skin of the domestic pig. J Invest Dermatol 1964;42(July):11–21.
[30] Wang XQ, Liu PY, Kempf M, Cuttle L, Chang AH, Wong M, et al. Burn healing is dependent on burn site: a quantitative analysis from a porcine burn model. Burns 2009;35(March (2)):264–9.
[31] Wang XQ, Kravchuk O, Liu PY, Kempf M, Boogaard CV, Lau P, et al. The evaluation of a clinical scar scale for porcine burn scars. Burns 2009;35(June (4)):538–46.
[32] Meyer W, Schwarz R, Neurand K. The skin of domestic mammals as a model for the human skin, with special reference to the domestic pig. Curr Probl Dermatol 1978;7:39–52.
[33] Sullivan TP, Eaglstein WH, Davis SC, Mertz P. The pig as a model for human wound healing. Wound Repair Regen 2001;9(March–April (2)):66–76.
[34] Luo T, Chen JX, Zhuo SM, Lu KC, Jiang XS, Liu QG. Visualization of collagen regeneration in mouse dorsal skin using second harmonic generation microscopy. Laser Phys 2009;19(March (3)):478–82 [article].